Proton NMR Conformational Study of an Annexin I Fragment: Influence of a Phospholipidic Micellar Environment

François Macquaire,† Françoise Baleux,‡ Tam Huynh-Dinh,‡ Dominique Rouge,† Jean-Michel Neumann,† and Alain Sanson*,†,§

Département de Biologie Cellulaire et Moléculaire, SBPM, URA CNRS 1290, CEN Saclay, 91191 Gif sur Yvette Cedex, France, and Unité de Chimie Organique, URA CNRS 487, Institut Pasteur, 28 rue du Dr Roux, 75724 Paris Cedex 15, France

Received February 1, 1993

ABSTRACT: A 32 residue peptide, Ac-AQWDADELRAAMKGLGTDEDTLIEILASRTNK, spanning the first helix–loop–helix motif of the second repeat of human annexin I, was synthesized and studied by standard 2D proton NMR and molecular modeling. The peptide was solubilized either in aqueous solution, in TFE–H_2O mixtures or in aqueous phospholipidic micellar solution. In pure aqueous solution, elements of helix secondary structure were observed. Addition of TFE led to a dramatic cooperative effect on the secondary structure with a very low transition midpoint indicative of the strong tendency of the peptide to form α helices. Only in the aqueous micellar solution was the full helix–loop–helix motif obtained, showing again the potency of a membrane-like micellar environment to initiate peptide secondary structures and even elements of tertiary structure. There were sufficient NMR data to perform molecular modeling of the structure of the annexin fragment solubilized in the presence of micelles. However, this structure showed a relatively high degree of flexibility, especially around the T17-D18 hinge at the end of the loop.

Annexins (lipocortins) belong to a new family of calcium-dependent membrane-binding proteins (Klee 1988; Pepinsky et al., 1988; Burgoyne & Geisow, 1989; Römisch & Paques, 1991). These proteins are expressed in various organisms including plants, and up to now, 12 elements of this family have been characterized. At the present time, the actual biological functions of the annexins remain unknown. As a result of numerous *in vivo* and *in vitro* observations, annexins have been assigned several possible functions, namely, inhibition of phospholipase A2, inhibition of coagulation factors, calcium buffering, cytoskeleton interactions, and functions in exocytosis and in synaptic vesicles traffic. A comprehensive review of annexin structures and functions will be found in *Annexins*, 1992, edited by S.E. Moss.

All these functions have a common prerequisite: the calcium dependent anchoring of the protein at a membrane interface with a strong specificity for phosphatidylserines. As with the function, the structure of the annexin–Ca^{2+}–phospholipid complex is still unknown. However, annexins probably constitute the first suitable model we can use for studying the biologically essential anchoring of the protein at a membrane surface. Given the level of our understanding of annexin biochemical and cellular functions, it is thus very important to gain an insight into the structure and dynamics of these proteins and of their complexes with calcium and phospholipids.

A crucial step was the elucidation of the crystal structure of annexin V (Huber et al., 1990a, 1990b, and 1992). In accordance with the primary structure consisting of four internal repeating units (twice four repeats in annexin VII), the tertiary structure is composed of four structurally homologous domains. The structural motif of each domain is a characteristic (helix–loop–helix)–helix–(helix–loop–helix) folding. Most of the calcium ligands, whenever present, are localized in the first loop. These domains might be functional units for calcium and phospholipid binding. The fact that the domains have most probably evolved from a small ancestral protein also supports this view. In this respect, annexins constitute a reliable model for NMR[1] studies. At the present time, the molecular weight of annexins (~35 kDa) precludes a detailed structural NMR investigation whereas the domains fulfill NMR spectroscopy requirements.

Our first objective is thus to investigate structure and dynamics of annexin domains and their complexes with calcium and phospholipids. Since the domains cannot be obtained by proteolysis, our approach is presently based on peptide synthesis. An 18-residue fragment corresponding to the consensus sequence of annexins was first studied (Macquaire et al., 1992a). In the present paper, we report structural data relative to a 32-residue fragment, Ac-AQWDADEL-RAAMKGLGTDEDTLIEILASRTNK, representing the first helix–loop–helix motif of the second repeat of human annexin I.

We studied the conformation of this annexin fragment solubilized in three solvent environments: in aqueous solution, in TFE–H_2O mixtures, and in an aqueous phospholipidic micellar solution. Such an approach is able to provide information on the folding process of a protein and contributes to our second objective, namely, a better understanding of the successive folding states associated with peptide elongation and the role of the environment in this process. In this respect, annexins are also interesting models because of their very high helix secondary structure content, the absence of β sheet and their unique folding. In the particular case of annexins that are cytosolic proteins and probably do not interact with endoplasmic reticulum during synthesis, the membrane-like environment is, *a priori*, not the relevant environment for studying the folding processes. However, the effect of such an environment is exemplary. In a recent paper (Macquaire

† Département de Biologie Cellulaire et Moléculaire.

‡ Unité de Chimie Organique.

§ Also from Université P. et M. Curie, 9 Quai Saint-Bernard, Bât. C, 75005 Paris, France.

[1] COSY, correlated spectroscopy; DG, distance geometry; DPC, dodecylphosphocholine; EDTA, ethylenediaminetetraacetic acid; NMR, nuclear magnetic resonance; NOE, nuclear Overhauser enhancement; NOESY, nuclear Overhauser enhancement spectroscopy; SA, simulated annealing.

0006-2960/93/0432-7244$04.00/0

et al., 1992b), we showed that a membrane-like interface was able to induce a specific secondary structure in a small peptide anchored within the interface. In the present paper, we report the influence of the same micellar environment on a peptide the size of which is larger than that of lipidic molecules. Our results demonstrate the ability of such an environment to complete secondary structures and induce elements of tertiary structure in a large protein fragment. Our work contributes to the scarce but increasing amount of results in this research field (Brown et al., 1982; Wider et al., 1982; Arseniev et al., 1985; Schiksnis et al., 1987; Olejniczak et al., 1988; O'Neil & Sykes, 1988; Inagaki et al., 1989; Karslake et al., 1990; Motta et al., 1991; Kohda & Inagaki, 1992).

MATERIALS AND METHODS

Synthesis of the Ac-AQWDADELRAAMKGLGTDEDT-LIEILASRTNK Peptide. The peptide was synthesized by the Merrifield solid-phase method (Merrifield, 1963) on an Applied Biosystems 430A synthesizer. The synthesis was performed using 0.5 mmol of Boc Lys(2-ClZ) Pam resin. Stepwise elongation of the peptide chain was done using the standard coupling protocols. To obtain the peptide in the N-terminal acetylated form, the peptide resin was treated with acetic anhydride using our own program.

Half of the peptide resin (1.3 g) was subjected to the low–high HF cleavage (Tam & Heath, 1983). After gel filtration on Bio-Gel P4, the peptide (283 mg) was purified on a Nucleosil 5-μm C18 300-Å semipreparative column, using a 20–35% linear gradient of acetonitrile in 50 mM ammonium acetate for 20 min at a 6 mL/min flow rate. The final purity of the peptide (99.9%) was checked on a Nucleosil 5-μm C18 300-Å analytical column, using a 20–60% linear gradient of the same eluents as above, at a 1 mL/min flow rate. The retention time was 11.68 min and the yield was 72 mg. Amino acid analysis was performed, after 6 N (5% mercaptoethanol) HCl, 110 °C, 20-h peptide hydrolysis, on a Beckman 6300 analyser and gave the following peptide composition: Ala, 5.0 (5); Asx, 4.8 (5); Glx, 3.9 (4); Gly, 2.0 (2); Ile, 1.8 (2); Lys, 1.8 (2); Leu, 3.9 (4); Met, 0.8 (1); Arg, 1.9 (2); Ser, 0.9 (1); Thr, 2.7 (3); Trp, ND. The integrity of the Trp residue was checked by UV absorption: 274 (shoulder), 279 (max), 289 nm (shoulder).

NMR Experiments. Free peptide (8 mg) was dissolved in 0.4 mL of 10 mM phosphate buffer containing 0.1 mM EDTA and lyophilized in either D_2O or 90:10 H_2O:D_2O. The pH was adjusted to 6.4. Standard 500- or 600-MHz two-dimensional phase-sensitive experiments (COSY, TOCSY, and NOESY; Wüthrich, 1986; Markley, 1989) were performed on Bruker AMX 500 and 600 spectrometers. A second set of 2D experiments was recorded for the peptide solubilized in various TFE:H_2O (D_2O) mixtures (from 2:98 to 36:64, vol/vol). Finally, a third sample of the annexin fragment was solubilized in a aqueous solution (under the same experimental conditions as above) containing 16 mg of deuterated dodecylphosphocholine micelles (MSD Isotopes) and a third set of NMR experiments were performed. In the latter case, the solution was sonicated for 10 min with a Branson sonicator.

In general, a total of 48 (COSY, TOCSY) or 80 (NOESY) transients were acquired with a recycling delay of 1 s. A total of 512 increments of 2K data points were collected for each 2D experiment yielding a digital resolution of 6 or 8 Hz/point in both dimensions after zero filling. Shifted squared sine-bell functions were used for apodization. NOESY spectra were recorded with mixing times of 80 and 160 ms (TFE and micelles) or 100, 200, and 300 ms (pure aqueous solution).

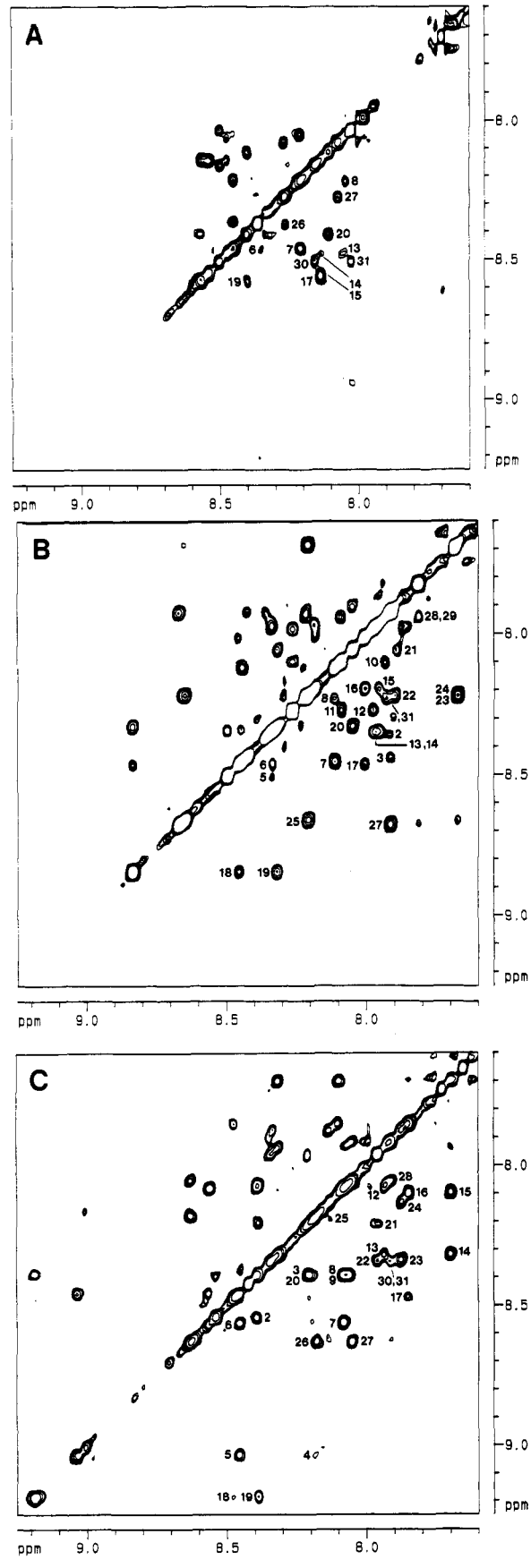

FIGURE 1: NH–NH region of the annexin fragment NOESY spectrum. (A) In pure aqueous solution (5 °C, mixing time of 300 ms); (B) in a 20:80 TFE:H_2O mixture (20 °C, mixing time of 160 ms); (C) in an aqueous micellar solution (20 °C, mixing time of 160 ms). The number located on one side of each cross peak labels the NH–NH correlation as follows: number 1 corresponds to the NH–NH (1, 2) NOE, number 2 to the NH–NH (2, 3) NOE, etc.

Table I

residue	chemical shift				
	NH	αH	βH	others	
(A) ^{1}H Chemical Shifts (ppm, TSP Reference) of the Annexin Fragment in Water, pH* = 6.4, T = 20 °C					
A_1	8.30	4.22		βCH$_3$ 1.27	
Q_2	8.29	4.29	1.96/1.86	γCH$_2$ 2.24/2.17	NH$_2$ 7.53/6.86
W_3	8.14	4.74	3.32/3.21	H^2 7.27 H^4 7.61	H^5 7.12
				H^6 7.22 H^7 7.48	NH 10.18
D_4	8.39	4.61	2.68/2.64		
A_5	8.35	4.10		βCH$_3$ 1.46	
D_6	8.36	4.51	2.76/2.73		
E_7	8.45	4.12	2.11/2.11	γCH$_2$ 2.37/2.26	
L_8	8.18	4.16	1.73/1.64	γCH *a*	δCH$_3$ 0.83/0.83
R_9	8.08	4.08	1.90/1.90	γCH$_2$ 1.74/1.62	δCH$_2$ 3.23/3.23
A_{10}	8.04	4.19		βCH$_3$ 1.48	
A_{11}	8.00	4.25		βCH$_3$ 1.46	
M_{12}	8.06	4.35	2.16/2.10	γCH$_2$ 2.68/2.55	
K_{13}	8.05	4.28	1.88/1.88	γCH$_2$ 1.55/1.49	δCH$_2$ 1.71/1.71
				εCH$_2$ 3.02/3.02	
G_{14}	8.44	3.99			
L_{15}	8.10	4.42	1.77/1.68	γCH 1.65	δCH$_3$ 0.94/0.90
G_{16}	8.50	4.05			
T_{17}	8.10	4.45	4.26	γCH$_3$ 1.21	
D_{18}	8.52	4.65	2.79/2.75		
E_{19}	8.57	4.17	2.10/2.00	γCH$_2$ 2.30/2.30	
D_{20}	8.39	4.57	2.74/2.71		
T_{21}	8.09	4.18	4.14	γCH$_3$ 1.26	
L_{22}	8.10	4.22	1.67/*a*	γCH *a*	δCH$_3$ 0.92/0.88
I_{23}	8.06	4.89	1.94	γCH$_2$ 1.91/1.25	γCH$_3$ 0.95
				δCH$_3$ 0.90	
E_{24}	8.12	4.21	2.08/2.08	γCH$_2$ 2.33/2.25	
I_{25}	8.19	3.97	1.95	γCH$_3$ 1.65/1.20	γCH$_3$ 0.90
				δCH$_3$ 0.86	
L_{26}	8.33	4.20	1.74/1.74	γCH 1.54	δCH$_3$ 0.84/0.84
A_{27}	8.26	4.29		βCH$_3$ 1.49	
S_{28}	8.05	4.44	2.99/2.99		
R_{29}	8.08	4.46	1.99/1.86	γCH$_2$ 1.75/1.71	δCH$_2$ 3.20/3.20
T_{30}	8.14	4.27	4.38	γCH$_3$ 1.26	
N_{31}	8.46	4.80	2.89/2.81		
K_{32}	7.99	4.18	1.85/*a*	γCH$_2$ 1.42/1.42	δCH$_2$ 1.71/1.71
				εCH$_2$ 3.03/3.03	
(B) ^{1}H Chemical Shifts (ppm, TSP Reference) of the Annexin Fragment in 20:80 TFE:H$_2$O, pH* = 6.4, T = 20 °C					
A_1	8.27	4.24		βCH$_3$ 1.25	
Q_2	8.36	4.32	1.99/1.88	γCH$_2$ 2.27/2.21	NH$_2$ 7.75/6.80
W_3	7.91	4.78	3.31/3.18	H^2 7.22 H^4 7.57	H^5 7.10
				H^6 7.18 H^7 7.44	NH 10.08
D_4	8.43	4.70	2.74/2.74		
A_5	8.49	4.10		βCH$_3$ 1.49	
D_6	8.34	4.51	2.84/2.69		
E_7	8.44	4.10	2.20/2.10	γCH$_2$ 2.24/2.27	
L_8	8.11	4.11	1.71/1.63	γCH 1.50	δCH$_3$ 0.81/0.81
R_9	8.22	3.98	2.00/2.00	γCH$_2$ 1.88/1.63	δCH$_2$ 3.30/3.25
A_{10}	7.94	4.17		βCH$_3$ 1.54	
A_{11}	7.92	4.19		βCH$_3$ 1.52	
M_{12}	8.26	4.21	2.17/2.03	γCH$_2$ 2.71/2.51	
K_{13}	7.98	4.23	1.97/1.97	γCH$_2$ 1.61/1.52	δCH$_2$ 1.76/1.76
				εCH$_2$ 3.03	
G_{14}	8.34	3.98			
L_{15}	7.96	4.42	1.85/1.78	γCH 1.63	δCH$_3$ 0.90/0.90
G_{16}	8.19	4.10/4.00			
T_{17}	8.01	4.54	4.19	γCH$_3$ 1.24	
D_{18}	8.46	4.76	2.89/2.83		
E_{19}	8.84	4.02	2.07/2.07	γCH$_2$ 2.35/2.35	
D_{20}	8.32	4.46	2.75/2.75		
T_{21}	8.05	4.04	4.23	γCH$_3$ 1.26	
L_{22}	7.90	4.06	1.81/1.65	γCH *a*	δCH$_3$ 0.90/0.90
I_{23}	8.21	3.68	2.00	γCH$_2$ 1.74/1.26	γCH$_3$ 0.96
				δCH$_3$ 0.91	
E_{24}	7.67	4.10	2.22/2.22	γCH$_2$ 2.43/2.32	
I_{25}	8.21	3.76	2.06	γCH$_2$ 1.86/1.10	γCH$_3$ 0.89
				δCH$_3$ 0.91	
L_{26}	8.65	4.03	1.89/1.82	γCH 1.47	δCH$_3$ 0.78/0.78
A_{27}	8.68	4.22		βCH$_3$ 1.54	
S_{28}	7.92	4.44	4.11/4.11		
R_{29}	7.81	4.45	2.07/1.93	γCH$_2$ 1.62/1.62	δCH$_2$ 3.15/3.15
T_{30}	7.94	4.34	4.41	γCH$_3$ 1.29	

Table I (Continued)

residue	chemical shift				
	NH	αH	βH	others	
(B) ^{1}H Chemical Shifts (ppm, TSP Reference) of the Annexin Fragment in 20:80 TFE:H_2O, pH* = 6.4, T = 20 °C					
N_{31}	8.24	4.82	2.90/2.84	NH_2 7.69/6.92	
K_{32}	7.91	4.23	1.88/1.79	γCH_2 1.44/1.44	δCH_2 1.71/1.71
				ϵCH_2 3.05	
(C) ^{1}H Chemical Shifts (ppm, TSP Reference) of the Annexin Fragment in Aqueous Micellar Solution, pH* = 6.4, T = 20 °C					
A_1	8.42	4.24		βCH_3 1.32	
Q_2	8.53	4.38	2.09/1.93	γCH_2 2.32/2.32	NH_2 7.66/6.91
W_3	8.39	4.65	3.23/3.23	H^2 7.30 H^4 7.52	H^5 6.99
				H^6 7.10 H^7 7.48	NH 10.4
D_4	8.18	4.77	2.88/2.80		
A_5	9.02	4.06		βCH_3 1.55	
D_6	8.46	4.51	2.88/2.68		
E_7	8.55	4.20	2.26/2.11	γCH_2 2.46/2.34	
L_8	8.07	4.17	1.84/1.75	γCH 1.59	δCH_3 0.95/0.91
R_9	8.39	3.98	2.03/2.00	γCH_2 1.90/1.65	δCH_2 3.31/3.28
A_{10}	8.06	4.19		βCH_3 1.57	
A_{11}	8.08	4.23		βCH_3 1.60	
M_{12}	8.07	4.16	2.23/2.18	γCH_2 2.73/2.52	ϵCH_3 2.02
K_{13}	7.93	4.27	2.00/2.00	γCH_2 1.66/1.56	δCH_2 1.79/1.79
				ϵCH_2 3.05/3.05	
G_{14}	8.31	4.05/3.97			
L_{15}	7.70	4.36	1.95/1.90	γCH 1.71	δCH_3 0.97/0.95
G_{16}	8.11	4.15/3.96			
T_{17}	7.85	4.59	4.06	γCH_3 1.17	
D_{18}	8.47	4.78	2.92/2.86		
E_{19}	9.19	3.97	2.11/2.11	γCH_2 2.36/2.32	
D_{20}	8.38	4.49	2.72/2.72		
T_{21}	8.21	4.06	4.33	γCH_3 1.31	
L_{22}	7.96	4.08	1.88/1.83	γCH 1.64	δCH_3 0.95/0.91
I_{23}	8.34	3.69	2.05	γCH_2 1.64/1.22	γCH_3 1.00
				δCH_3 0.95	
E_{24}	7.88	4.16	2.22/2.22	γCH_2 2.42/2.34	
I_{25}	8.13	3.85	2.09	γCH_2 1.95/1.23	γCH_3 0.96
				δCH_3 0.92	
L_{26}	8.18	4.10	1.89/1.82	γCH 1.54	δCH_3 0.96/0.91
A_{27}	8.62	4.21		βCH_3 1.53	
S_{28}	8.05	4.42	4.09/4.09		
R_{29}	7.91	4.48	2.09/1.94	γCH_2 1.85/1.79	δCH_2 3.23/3.23
T_{30}	7.91	4.42	4.33	γCH_3 1.27	
N_{31}	8.35	4.83	2.92/2.83	NH_2 7.74/7.00	
K_{32}	7.95	4.20	1.88/1.78	γCH_2 1.45/1.45	δCH_2 1.72/1.72
				ϵCH_2 3.05/3.05	

[a] Ambiguous.

Data were processed using either UXNMR (Bruker) or FELIX (Hare Research Inc., Woodinville, WA) software.

Distance Geometry/Simulated Annealing (DG/SA) Calculations. Peptide structures were generated from experimental NMR data using the DSPACE program (Hare Research Inc., Woodinville, WA) running on a Sparcstation 2 (Sun Microsystems). This software combines distance geometry and simulated annealing (DG/SA) algorithms (Summers et al., 1990).

RESULTS AND DISCUSSION

NMR Data for the Annexin I Fragment in Pure Aqueous Solution. The annexin fragment was first solubilized in a 90:10 H_2O:D_2O solution. Sequential assignment of peptide resonances was achieved from COSY, TOCSY, and NOESY spectra according to the standard methods. A NOESY spectrum (NH–NH region) is shown in Figure 1A. The complete set of chemical shifts is listed in Table I-A and Figure 2A gives the NOE and J data measured at 20 °C. At 5 °C, the number of NH–NH (i, i + 1) NOEs observed was significantly greater than those detected at 20 °C and these NOEs were added to Figure 2A. As far as the other NOESY regions are concerned, the low temperature experiment did not reveal additional data and moreover, complicated the interpretation because of increased linebroadening.

Short linear peptides do not usually present stable conformations in aqueous solution. However a limited number of examples have shown that canonical conformational states, specially helices and turns, may be significantly populated in the case of protein fragments [see Wright et al. (1988) and Dyson and Wright (1991) for a review]. Moreover, these conformational states were often representative of the folded conformation of the whole protein. Our 32-residue annexin fragment represents a new example. Indeed, a few but characteristic medium range (i, i + 3) and (i, i + 4) NOEs were observed within the D6-K13 segment, on one hand, and within the D20-A27 segment, on the other hand (Figure 2A), indicating the presence of a partial secondary structure. These NOE correlations *may* be consistent with a helix conformational state extending approximately from D6 to K13 and from D20 to A27. The $J_{\alpha N}$ values (Figure 2A) measured for the central residues in both segments were less than 6 Hz, in agreement with a preferential helical structure. However, the complete network of (i, i + 3) and (i, i + 4) NOEs expected for a *unique* α helix conformation extending over the full D6-K13 and D20-A27 segments was far from being observed.

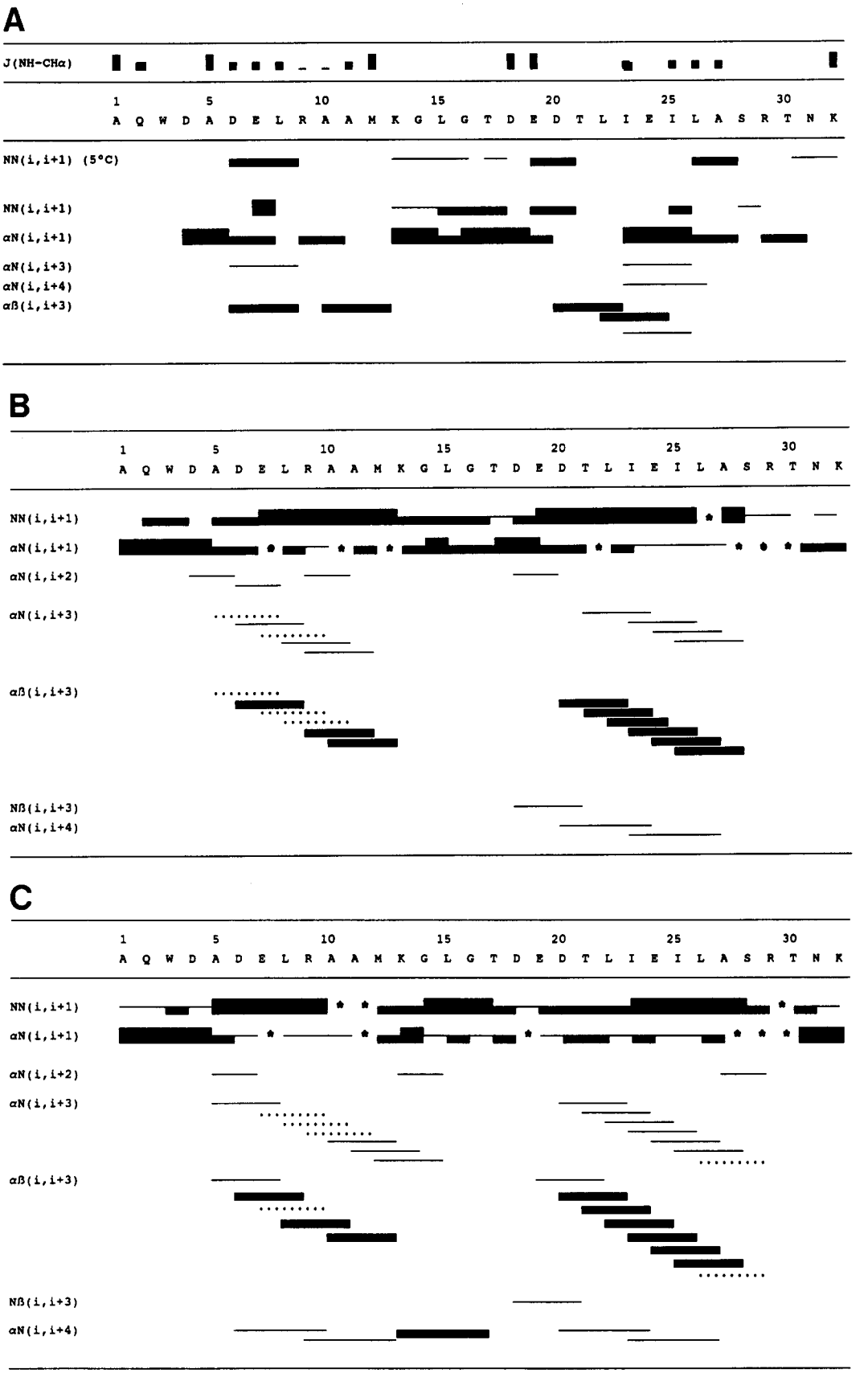

FIGURE 2: Interproton NOEs characteristic of the annexin fragment secondary structure in pure aqueous solution (A), in a 20:80 TFE:H_2O mixture (B) and in an aqueous micellar solution (C) at 20 °C. An approximate representation of the NOE relative intensities is given by the vertical bars. Overlapping and therefore ambiguous cross peaks are indicated by an asterisk or a dashed line. For the peptide solubilized in pure aqueous solution, several $J_{\alpha N}$ values were measured and are schematically given in Figure 2A as follows: —, ▬, and ■ symbols correspond to J values less than 4 Hz, ranged between 4 and 6 Hz and ranged between 6 and 8 Hz, respectively. Sequential NH–NH NOEs observed at 5 °C are also included in Figure 2A.

A closer inspection of the data revealed significant differences in the conformational state of the two segments of the protein fragment. Including the NH–NH (i, i + 1) NOEs, obtained at 5 °C (Figure 2A), the D6-R9 segment exhibited

a set of NOE and $J_{\alpha N}$ data characteristic of a complete helix turn. This helix turn is observed in water probably because of a possible D6-R9 stabilizing salt bridge. Indeed, the occurrence of a salt bridge was demonstrated for the peptide solubilized in the presence of TFE or micelles (see below). Such a helix turn is an important structural feature and can be considered as an essential nucleating site in the initial steps of the protein folding process. The additional A10-K13 $\alpha\beta$ ($i, i + 3$) contact and the small $J_{\alpha N}$ value measured for the two consecutive A10 and A11 alanine residues also indicated the presence of a folded structure in the C-terminal part of the segment, the more that alanine is known to be an efficient helix promoter. However, because of the absence or degeneracy of the characteristic NH–NH ($i, i + 1$) NOEs, it was difficult to estimate how populated is the helix structure that could propagate from the D6-R9 structured cluster.

As regards the E19/D20-A27 segment, the data were contradictory since there was strong evidence of helix structure as indicated by the five ($i, i + 3$) or ($i, i + 4$) NOE connectivities together with an absence of several characteristic NH–NH ($i, i + 1$) NOEs within the same segment (T21-I25) (Figure 2A). Indeed, the intense sequential αN NOEs observed between I23 and L26 and the absence, even at 5 °C, of sequential NH–NH NOEs between I23 and I25 are not consistent with a helix structure. To reconcile these data, we suggest the following interpretation. The (D20-A27) segment is rather amphiphilic and the L22, I23, I25, and L26 residues constitute a highly hydrophobic cluster. These residues tend to reduce their interaction with water molecules by folding or condensing into a hydrophobic core. The consequence is a collapse of the helix structure which tends to form in the E19/D20-I23 segment, as judged by the characteristic ($i, i + 1$) and ($i, i + 3$) connectivities. The medium range NOEs observed in the I23-A27 segment would thus result from the particular folding of this hydrophobic core. In addition, it can be seen that residues 23 and 25 are β-branched amino acids which are known to be less favorable for the stability of the helix structure (Dao-Pin et al., 1990; Lyu et al., 1991).

As regards the K13/G14-D18 segment, only sequential NH–NH and CHα–NH ($i, i + 1$) correlations were obtained (Figure 2A). Such a set of NOE connectivities observed in a peptide segment containing glycine residues could be indicative of local β-turn structures. However the methylene protons of both G14 and G16 glycine residues were magnetically equivalent (Table IA). The NOE pattern of this segment most probably reflected a conformational equilibrium between turnlike structures.

NMR Data for the Annexin I Fragment in TFE:H_2O Mixtures. TFE is well-known to stabilize the helix structure and principally this canonical secondary structure. The TFE effect was clearly demonstrated for the annexin fragment. Comparison of Figure 1A with Figure 1B shows the dramatic effect of the addition of TFE (TFE:H_2O 20:80) on the annexin fragment NOESY spectrum (amide proton region). Indeed, on increasing the TFE concentration, the spectral interval containing the NH signals was progressively extended from 0.6 ppm in pure aqueous solution to 1.2 ppm in a TFE:H_2O 20:80 mixture. Above this ratio, the spectrum was no longer modified (see also Figure 3). The complete signal assignment of the peptide solubilized in various TFE:H_2O solutions was achieved from COSY, TOCSY, and NOESY experiments and the proton chemical shifts measured for a TFE:H_2O 20:80 mixture at 20 °C are listed in Table IB. Figure 2B gives the NOE data (TFE:H_2O 20:80, 20 °C). Coupling constants could not be measured because of too broad line widths.

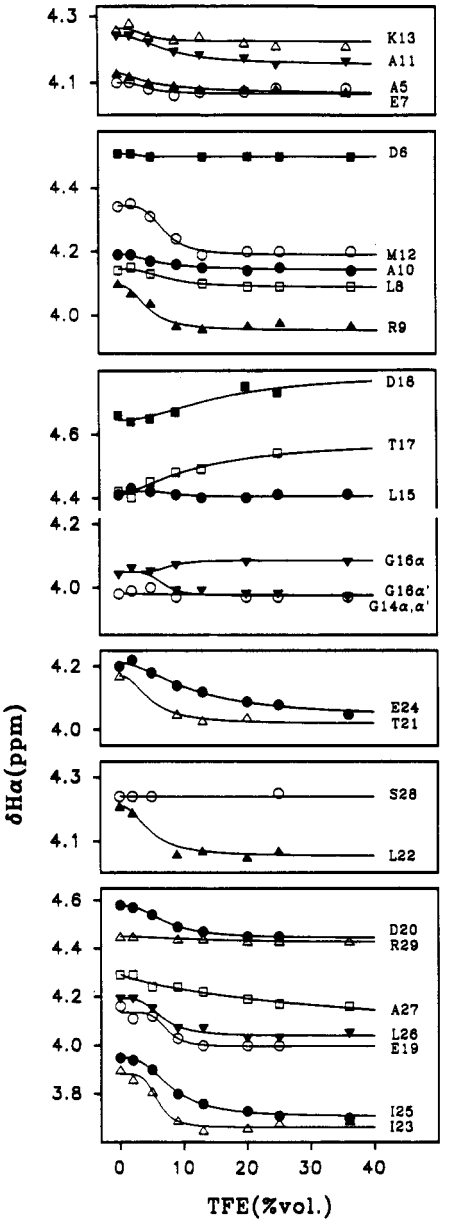

FIGURE 3: Hα chemical shifts (in ppm) versus TFE percentage (in volume) of the annexin fragment solubilized in TFE:H_2O solutions.

The tendency of the first previously delineated segment (D6-K13) to form a helix structure was clearly demonstrated by the TFE effect. The resulting NOE pattern exhibited a full set of sequential NH–NH connectivities, a full set of medium or weak αN connectivities and six unambiguous αN and $\alpha\beta$ ($i, i + 3$) connectivites (Figure 2B). The D6-R9 salt bridge, previously suggested for the peptide in pure aqueous solution, was clearly revealed by a $\alpha\delta$ (D6, R9) NOE correlation (not shown in Figure 2B) and the significant magnetic nonequivalence of the D6 (Hβ, Hβ') and R9 (Hδ, Hδ') signals (Table IB). The (D6-K13) segment is rather hydrophilic, and the TFE effect is probably to reduce the water activity around the helix hydrogen bond network and thus to increase the overall stability of the structure. As regards the second delineated segment (E19/D20-A27), the presence of TFE dramatically increased the number of interresidue NOEs: an undisrupted set of $\alpha\beta$ ($i, i + 3$) contacts from the D20 α proton up to the S28 β protons was observed together with a regular set of αN ($i, i + 3$) connectivities, strong NH–NH ($i, i + 1$) and medium or weak αN ($i, i + 1$) NOEs (Figure 2B). All these NMR data are fully consistent with

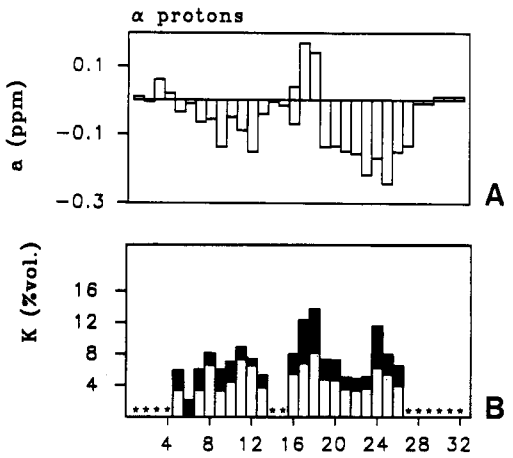

FIGURE 4: (A) Differences (a, in ppm) between the Hα chemical shift of the annexin fragment solubilized in H_2O and in 20:80 TFE:H_2O as a function of residue number. (B) Transition midpoint (K, in TFE percentage) measured from the curves of Figure 3, as a function of residue number; for each residue, the filled region gives the approximate accuracy of the measurement. An asterisk indicates a residue whose the Hα variation (vs TFE%) is not significant or not sigmoidal.

a well-defined helix structure extending from E19 to S28. According to our previous analysis concerning the hydrophobic cluster of this segment, the TFE effect could be, in this case, the hydrophobic solvation of the aliphatic residues, which relaxes the local energy of the peptide and allows the completion of the helix structure.

Addition of TFE also led to a conformational change within the K13-E19 segment as revealed by the magnetic nonequivalence of the G16 Hα and Hα' signals (Figure 3 and Table IB), and αN (18, 20) NOE, and the Nβ (18, 21) NOE (Figure 2B). The Nβ (18, 21) correlation appears unusual for a disordered fragment and rather suggests a break in the peptide backbone at the residue D18 which thus may be considered as the transition residue between the K13–E19 segment and the second helix. The absence of (18, 21) and (19, 22) αN and $\alpha\beta$ NOEs could result from the lower stability of the first helix turn. Finally, no long-distance NOE, such as helix–helix contacts, was detected.

A better understanding of the stabilizing effect induced by the presence of TFE was attempted by a detailed analysis of the Hα chemical shift variation as a function of the TFE concentration (Figure 3). The cooperative effect of TFE was clearly revealed by the sigmoidal form of the curves related to residues involved in a secondary structure. The chemical shift of residues located in both helices decreased with increasing TFE concentration. Such negative variations of δ(Hα) associated with helix-structure build up were in agreement with the now well-established conformational dependence of the Hα chemical shifts on secondary structure (Szilagyi & Jardetzky, 1989; Pastore & Saudek, 1990; Wishart et al., 1991, 1992; Jiménez et al., 1992). In contrast, the δ(Hα) of the G16–D18 fragment exhibited positive variations generally ascribed to β structure formation. In any case, these variations, associated with the previously mentioned chemical shift and NOE data, reflect a tendency of the G16-D18 segment to adopt a particular structure. In addition, the sigmoidal variations of δ(Hα) were analyzed in terms of maximum amplitude a (ppm) and transition midpoint K (TFE % v/v) as a function of residue number (Figure 4). Qualitative information can be deduced from these data. First, the amount of TFE necessary to induce maximum stabilization was rather low, i.e., less than 20% v/v TFE, for most of the residues in

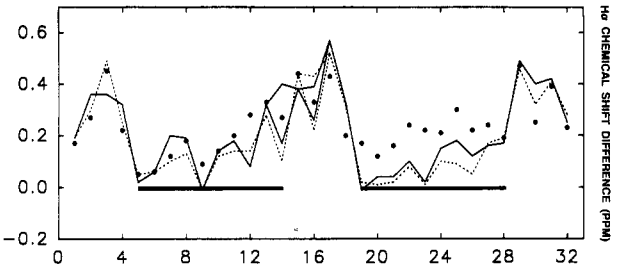

FIGURE 5: Chemical shift differences (in ppm) $\Delta\delta_\alpha = \delta(H\alpha)_{obs} - \delta(H\alpha)_{helix}$ (see text) for the residues of the annexin fragment solubilized in pure aqueous solution (●), in 20:80 TFE:H_2O mixture (dashed line) and in aqueous micellar solution (solid line) at 20 °C, as a function of residue number. The two horizontal bold lines refer to the two helix segments identified by the NOE data.

both helix segments (the average midpoint is about 6% TFE). Usually, the maximum stabilizing effect of TFE is reached at higher concentrations, 30–50% v/v. This point can be considered as a confirmation of the strong tendency of the annexin fragment to adopt secondary helix structure, even in pure aqueous solution. The midpoint K did not strongly vary along the sequence and did not indicate, at this level of investigation, any specific site of interaction of TFE with the peptide. The presence of TFE rather uniformly affected the peptide structure. Second, as regards the amplitude of δ-(Hα) variations (Figure 4A), a significant difference between the first and second helix segment was observed. The variation amplitude, a, was definitely smaller within the first segment than within the second one. To explain this difference the alternative was that, either TFE had a less stabilizing effect on the first helix, or the first helix was intrinsincally more stable than the second helix in pure aqueous solution. We favor the second hypothesis on the basis of already mentioned data (NOE and J(NH–CHα)) and on the chemical shift data of Figure 5 which are discussed in a forthcoming section.

NMR Data for the Annexin I Fragment Solubilized in Aqueous Solution Containing Phospholipidic Micelles. A NOESY spectrum (NH–NH region) of the annexin fragment solubilized with deuterated dodecylphosphocholine micelles (recorded at 20 °C with a mixing time of 160 ms) is shown in Figure 1C. Table IC lists the amino acid chemical shifts measured at 20 °C and Figure 2C gives the NOE data indicative of the secondary structure. Comparison of Figures 1A and 2A (pure aqueous solution) with Figures 1C and 2C shows the dramatic effect of the micellar environment and reflects a strong interaction of the annexin fragment with the phospholipidic micelles. In contrast, the effects of TFE and micelles (Figure 2B,C) on the peptide secondary structure were close although not identical. The data relative to the annexin fragment solubilized in the presence of micelles is thus compared, in the following discussion, to those obtained in the presence of TFE (20:80 TFE:H_2O).

First, we noticed an increase of the spectral interval containing the amide proton resonance (+0.3 ppm between the spectra of Figure 1B,C) and further ($i, i + 3$) and ($i, i + 4$) NOEs in the presence of micelles, which enabled us to define more precisely both helix domains (Figure 2C). The first helical domain can be extended from A5 to G14 and furthermore, the characteristic αN (13, 15) contact, the strong αN (13, 14) NOE, and the G14 Hα, Hα' magnetic non-equivalence (Table IC) suggested that G14 probably caps the first helix at the C end with a 3_{10} helix half-turn. This was confirmed by DG/SA calculations (see below). Second, the meaningful Nβ (18, 21) NOE, previously detected in the presence of TFE, was also observed and confirms D18 as the

Table II: $(i, i + 4)$ and $(i, i + 5)$ Connectivities within the M12-L22 Segment for the Peptide in the Micellar Solution[a]

αN (M12,T17) w	γβ (T17,T21) w
αγ (M12,T17) w	Nδ′ (T17,L22) w
εγ (M12,T17) s	γδ (T17,L22) w
αN (K13,T17) m	

[a] NOE intensities: weak (w); medium (m); strong (s).

transition residue between the second helix and the G14-T17 segment. In the presence of micelles, the latter segment clearly exhibited stong elements of secondary structure, i.e., the magnetic inequivalence of α protons for both glycine residues and the αN (13, 17) NOE contact.

However, the most striking difference between the TFE and micelle effects was that, in the presence of micelles, a further $(i, i + 3)$, $(i, i + 4)$, $(i, i + 5)$ NOE network spanning the M12-L22 segment and thus connecting the two helices was found (Table II). These new data reflected a folding of the intermediate G14-T17 segment into a surprisingly well-structured loop. As demonstrated below by using molecular modeling, the peptide folded into a rather well defined helix–loop–helix structure close to that found for the corresponding peptide in the native annexin V protein. This folding, which tends to bring together two elements of secondary structure (α helix), has to be considered as a tertiary-like structure. The ability of phospholipidic micelles to induce secondary structure was demonstrated for a number of peptides (see references cited at the end of the Introduction) especially in the case of amphipathic helices. However, to our knowledge, no example of tertiary-like structures induced by micelles has been published.

At the present time, we have no experimental data that could explain the mechanism of the micelle-induced folding. Several models can be assumed. A possible alternative can be proposed: (i) the peptide anchors at the micelle surface which merely restricts the peptide conformational space; (ii) the tertiary folding of the peptide generates an apolar face (L8, A11, M12, L22, I23, I25, L26) which is solvated by the micellar hydrophobic environment required for the peptide structure stabilization. Schematically, the first case corresponds to the classical picture of amphipathic peptides bound to micelles while the second, which implies an asymmetrical distribution of the lipid molecules around the peptide, in some way refers to detergent-solubilized membrane proteins. Whereas we have no serious arguments in favor of any model, the second model is, of course, rather attractive in so far as the micellar environment would thus mimic the hydrophobic core of the whole protein and allow a complete folding of the peptide.

Finally, the NOE data were sufficiently numerous for DG/SA calculations to be performed in order to precisely specify the average structure of the annexin fragment in the presence of micelles. However, before describing these results, it is worthwhile discussing in the following section the relationship between Hα chemical shifts and secondary structure.

Hα Chemical Shifts and Secondary Structure. The conformational dependence of the Hα chemical shifts, δ(Hα), is now well established (Szilagyi & Jardetzyk, 1989; Pastore & Saudek, 1990; Wishart et al., 1991, 1992; Jiménez et al., 1992). Figure 5 shows, for each residue and for various environments, the difference ($\Delta\delta_\alpha$) between the observed δ(Hα) value (Table I) and that corresponding to a standard helix form. The standard helix chemical shifts are the average values derived by Wishart et al. from a set of NMR studies (Wishart et al., 1991). The use of helix δ(Hα) data instead of coil δ(Hα) data as a reference seemed more appropriate inasmuch as the helix form is a well-characterized structure exhibiting only small local variations in contrast with the rather ill-defined coil structure.

Comparing the three $\Delta\delta_\alpha$ curves corresponding to the three different environments led to the following observations. The curves obtained for the peptide solubilized in the presence of TFE and in the presence of micelles are quite similar. Both curves reflect the existence of the two helix segments revealed by the NOE data. The beginning of both helices are dramatically marked ($\Delta\delta_\alpha(A5) \approx \Delta\delta_\alpha(E19) \approx 0$). Moreover, as already described by Jimenez et al. (Jimenez et al., 1992), the two curves exhibit pseudo-oscillations suggesting the $(i, i + 4)$ helix periodicity; this is particularly clear for the first helix turn of both helices (A5-R9, E19-I23). Beside these variations, we noticed, especially in the case of the second segment, that the $\Delta\delta_\alpha$ values statistically increased on going from the N-terminal residue toward the C-terminal residue of the helices. Linear regression performed using the $\Delta\delta_\alpha$ values of the A5-G14 region on one hand and the E19-S28 region on the other hand gave two slopes surprisingly close. The progressive increase of the $\Delta\delta_\alpha$ values was also observed in other $\Delta\delta_\alpha$ curves corresponding to helix structures (van der Graaf et al., 1991; Gao et al. 1991; Jiménez et al., 1992; Sönnichsen et al., 1992). The physical basis for this slope, that seems to be a characteristic feature of medium length helices, is not understood. In the A5-G14 segment, the $\Delta\delta_\alpha$ distribution of the peptide solubilized in pure aqueous solution partly fitted the curves corresponding to the TFE and micellar environments and significantly deviated from the latter ones in the E19-S28 region. Therefore, the $\Delta\delta_\alpha$ values indicated a difference in average structures between these two segments. In this respect, the chemical shift data correlated with the NOE data.

However, it is worthwhile noting that chemical shifts represent population-weighted averaged data over the whole conformational ensemble explored by the peptide at a rate typically faster than a few ms^{-1}. NOE data are also population-weighted, but, at variance with chemical shift data, over a conformational ensemble restricted to conformations that keep a given proton pair at a distance smaller than about 0.4 nm within the suitable time scale. In this respect, the rather small differences in chemical shift for the A5-G14 segment between the three solvents would, *a posteriori*, indicate that the helix or helixlike conformations of this segment are highly populated in pure aqueous solution.

Molecular Modeling of the Annexin I Fragment in the Presence of Micelles. As mentioned above, the experimental data available for a description of the annexin fragment tertiary structure in the presence of micelles concerned the M12-L22 segment, which, from this standpoint, constitutes the essential part of the peptide conformation. Therefore, we concentrated our attention on the R9-E34 sequence and limited the extensive DG/SA calculations to this region. Indeed, on one hand, the helix conformation of both (A5-G14) and (D18-S28) segments were experimentally well determined and, on the other hand, the N- and C-terminal (A1-D4), (T30-K32) segments exhibited no NOEs related to either a secondary or tertiary structure. Nevertheless, calculations restricted to both helix domains (data not shown) were performed without hydrogen bond constraints and confirmed the consistency of the NOE data. It has be be pointed out that (i) the second helix segment of the annexin I fragment remarkably coincides with the corresponding helix of the annexin V crystalline structure and (ii) the first helix segment starts at D4 instead of A1,

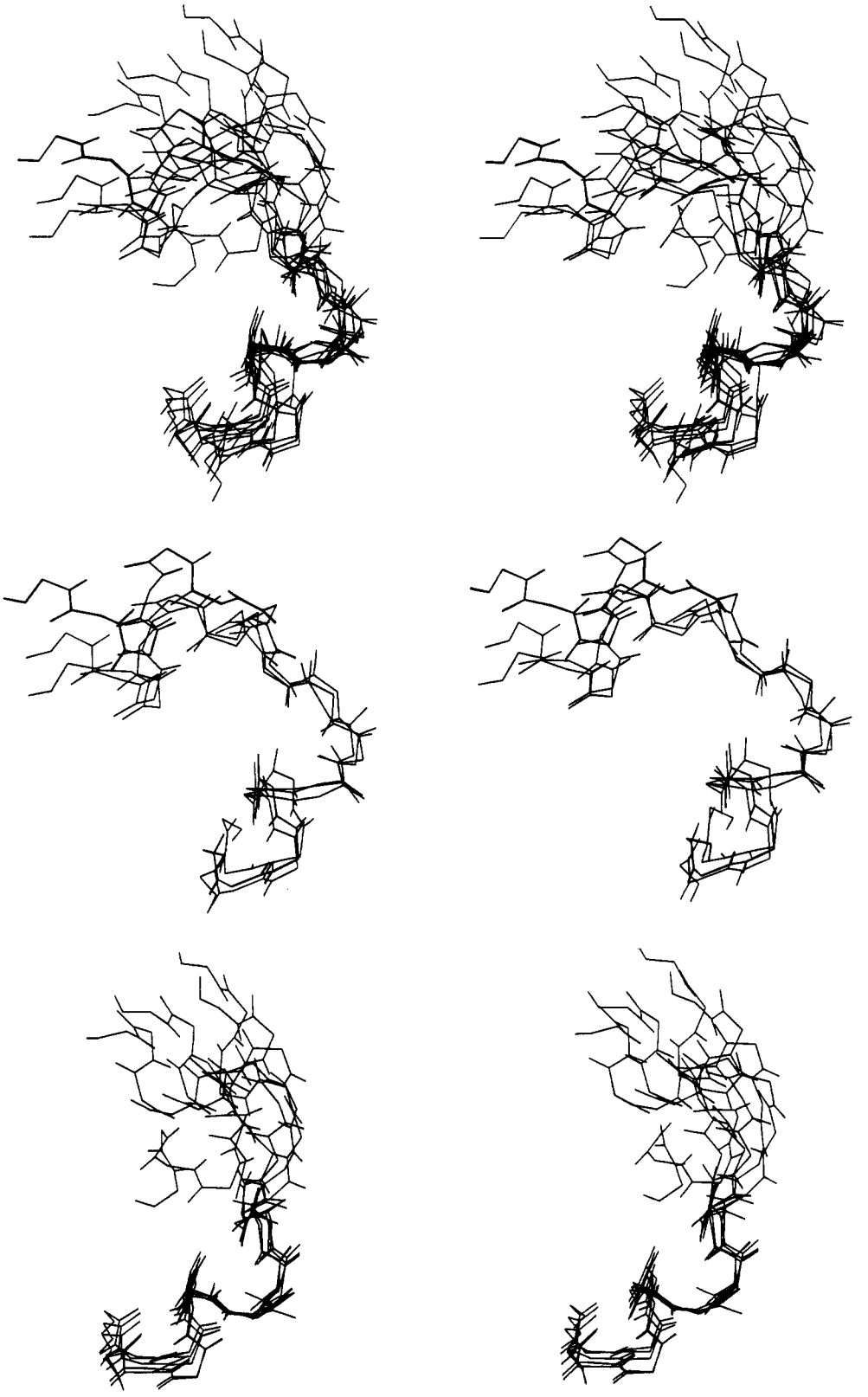

FIGURE 6: Superimposed DG/SA structures of the annexin fragment using NOE constraints obtained for the peptide solubilized in an aqueous micellar solution. Only the backbone and amide atoms extending from R9 to E24 are shown. The superpositioning (RMSD fit) was based on the backbone atoms of the K13-T17 fragment, i.e., the loop motif. The nine selected structures (A, top) can be separated into two families (B, middle) and (C, bottom) according to the relative orientation of the two helix axes (C terminal, top; N terminal, bottom).

probably because Asp is a much stronger helix signal residue than Ala (Presta & Rose 1988; Richardson & Richardson, 1988).

A set of 120 distance constraints were collected from the NOE data relative to the R9-E24 region and constituted the experimental constraint file. In addition, three hydrogen bonds (R9-K13, E19-I23, D20-E24) were included in this file, in order to save computation time. Figure 6A shows a superimposition of nine selected structures. The selection was performed as follows: (i) a first set of 45 structures was retained on the basis of the average energy value, (ii) structures exhibiting local energy peaks were then discarded, and (iii)

finally, the structures were sorted according to the quality of their Ramachandran plots with respect to a recent analysis (Morris et al., 1992).

The DG/SA calculations confirmed (i) G14 as the C-cap of the first helix because of the obvious possibility of a (i, i + 3) hydrogen bond between A11 and G14, revealed by the G14 position with respect to the helix and the G14 carbonyl–A11 NH distance and (ii) D18 as the first and N-cap residue of the second helix since the obtained structures enable a (i, i + 4) D18-L22 hydrogen bond and the range of D18 (ϕ, ψ) values tends to place the D18 side chain on top of the helix.

As shown in Figure 6B,C, the nine selected structures could be separated into two sets according to the relative orientation of the two helix segments. Such a duality reflected the scarcity of long distance NOEs which did not allow DG/SA calculations to select the actual tertiary structure of the peptide. This could result from a helix–helix arrangement involving ^{1}H–^{1}H distances mainly greater than 0.4 nm and/or from an intrinsic flexibility around the T17-D18 hinge.

Comparison with the Annexin V Crystal Tertiary Structure. One of the DG/SA structure families (Figure 6B) shows a helix–loop–helix folding of the annexin I fragment surprisingly close to that found in annexin V crystals, in particular as regards the relative direction of the two helix axes. Interestingly, the folding of the G14-T17 loop was quite conserved over the various structures of both sets and, on average, was also quite similar to that of the calcium-free annexin V crystals. Actually, the calcium-free loops of the annexin V crystalline form are apparently not better ordered (A. Bentley, private communication). A characteristic feature of the loop structure in the annexin I fragment is that the G14–L15–G16 segment adopts a planar conformation situated in the axis of the first helix, mimicking a pseudo partial helix turn. The reversal of the peptide backbone, achieving the connection to the second helix, occurs at the T17-D18 hinge in agreement with the annexin V structure.

CONCLUSION

We have synthesized and studied by proton NMR spectroscopy the first 32-residue fragment of the second repeat of human annexin I. This fragment is representative of the characteristic helix–loop–helix motif of annexins. Comparing the effects of the various solvents used in this study, we can summarize our results as follows. In pure aqueous solution, the annexin I fragment exhibits elements of structure in the two segments corresponding to helices in the native annexin V protein. In the first segment, the key structure is a helix turn, that is probably salt bridge stabilized, which provides this segment a large helix content. The second segment seems to fold into a rather uncharacterized structure around the cluster made by four hydrophobic residues. In the presence of TFE:H_2O mixtures and in a micellar aqueous solution, the two helix domains are strongly stabilized. Whereas the stabilizing effect of the water–TFE homogeneous mixed solvent is limited to the secondary helix structure, the heterogeneous micellar solution also induces an additional tertiary-like folding.

The intrinsically flexible annexin I fragment is able to adopt, in the presence of micelles, a helix–loop–helix tertiary structure close to that observed in the annexin V crystal structure. However, in our case, the effective mechanism for the action of micelles on the peptide structure, remains unknown although several hypotheses can be suggested. This question must now be addressed with specifically designed experiments. From a more general stand point, annexin fragments clearly constitute good models for studying protein folding and an effort is presently being made in our laboratory, in this direction. In the specific case of annexins, our results also confirm the relevance of protein fragment studies and enable an NMR study of the elementary functional annexin–calcium–phospholipid complex. For this purpose, a 70-residue fragment representing the second domain of annexin I was synthesized and should provide us with a good model for investigating the molecular mechanisms of the biologically important protein anchoring at the membrane surface.

REFERENCES

Annexins, 1992, Moss, S. E., Ed., Portland Press, London.

Arseniev, A. S., Barsukov, V. F., Lomize, A. L., & Ovchinnikov, Y. A. (1985) *FEBS Lett. 186*, 168–174.

Brown, L. R., Braun, W., Kumar, A., & Wüthrich, K. (1982) *Biophys. J. 37*, 319.

Burgoyne, R. D., & Geisow, M. J. (1989) *Cell Calcium 10*, 1–10.

Dao-Pin, S., Baase, W. A., & Matthews, B. W. (1990) *Proteins 7*, 198–204.

Dyson, H. J., & Wright, P. E. (1991) *Annu. Rev. Biophys. Biophys. Chem. 20*, 519–538.

Gao, Y., Veitch, N. C., & Williams, R. J. P. (1991) *J. Biomol. NMR 1*, 457–471.

Huber, R., Römisch, J., & Paques, E. P. (1990a) *EMBO J. 9*, 3867–3874.

Huber, R., Schneider, M., Mayr, I., Römisch, J., & Paques, E. P. (1990b) *FEBS Lett. 275*, 15–21.

Huber, R., Berendes, R., Burger, A., Schneider, M., Karshikov, A., Luecke, H., Römisch, J., & Paques, E. (1992) *J. Mol. Biol. 223*, 683–704.

Inagaki, F., Shimada, I., Kawaguchi, K., Hirano, M., Terasawa, I., Ikura, T., & Go, N. (1989) *Biochemistry 28*, 5985–5991.

Jiménez, M. A., Blanco, F. J., Rico, M., Santoro, J., Herramz, J., & Nieto, J. L. (1992) *Eur. J. Biochem. 207*, 39–49.

Kaori, W., Akihiko, O., Tatsuo, M., Masanao, O., & Tsutomu, H. (1992) *Biochemistry 31*, 5654–5660.

Karslake, C., Piotto, M. E., Pak, Y. K., Weiner, H., & Gorenstein, D. G. (1990) *Biochemistry 29*, 9872–9878.

Klee, C. B. (1988) *Biochemistry 27*, 6645–6653.

Kohda, D., & Inagaki, F. (1992) *Biochemistry 31*, 677–685.

Lyu, P., Sherman, J. C., Chen, A., & Kallenbach, N. R. (1991) *Proc. Natl. Acad. Sci. USA 88*, 5317–5320.

Macquaire, F., Baleux, F., Huynh-Dinh, T., Neumann, J. M., & Sanson, A. (1992a) *Int. J. Pep. Prot. Res. 39*, 117–122.

Macquaire, F., Baleux, F., Giaccobi, E., Huynh-Dinh, T., Neumann, J. M., & Sanson, A. (1992b) *Biochemistry 31*, 2576–2582.

Markley, J. L. (1989) *Methods Enzymol. 176*, 12–63.

Merrifield, R. B. (1963) *J. Am. Chem. Soc. 85*, 2149–2154.

Morris, A. L., MacArthur, M. W., Hutchinson, E. G., & Thornton, J. M. (1992) *Proteins 12*, 345–364.

Motta, A., Pastore, A., Goud, M. A., & Castiglione Morelli, M. A. (1991) *Biochemistry 30*, 10444–10450.

Olejniczak, E. T., Gampe, R. T., Rockway, T. W., & Fesik, S. W. (1988) *Biochemistry 27*, 7124–7131.

O'Neil, J. D. J., & Sykes, B. D. (1988) *Biochemistry 27*, 2753–2762.

Pastore, A., & Saudek, V. (1990) *J. Magn. Reson. 90*, 165–176.

Pearson, R. H., & Pascher, I. (1979) *Nature (London) 281*, 499–501.

Pepinsky, R. B., Tizard, R., Mattaliano, R. J., Sinclair, L. K., Miller, G. T., Browning, J. L., Chow, E. P., Burne, C., Huang, K. S., Pratt, D., Wachter, L., Hession, C., Frey, A. Z., & Wallner, B. P. (1988) *J. Biol. Chem. 263*, 10799–10811.

Presta, L. G., & Rose, G. D. (1988) *Science 240*, 1632–1641.

Richardson, J. S., & Richardson, D. C. (1988) *Science 240*, 1648–1652.

Römisch, J., & Paques, E. P. (1991) *Med. Microbiol. Immunol. 180*, 109–126.

Schiksnis, R. A., Bogusky, M. J.; Tsang, P., & Opella, S. J. (1987) *Biochemistry 26*, 1373–1381.
Sönnichsen, F. D., van Eyk, J. E., Hodges, R. S., & Sykes, B. D. (1992) *Biochemistry 31*, 8790–8798.
Summers, M. F., South, T. L., Kim, B., & Hare, D. R. (1990) *Biochemistry 29*, 329–340.
Szilagyi, L., & Jardetzky, O. (1989) *J. Magn. Reson. 83*, 441–449.
Tam, J. P., & Heath, W. F. (1983) *J. Am. Chem. Soc. 105*, 6442–6447.
Van der Graaf, M., van Mierlo, C. P. M., & Hemminga, M. A. (1991) *Biochemistry 30*, 5722–5727.
Von Heijne, G. (1990) *J. Membr. Biol. 115*, 195–201.
Wider, G., Lee, K. H., & Wüthrich, K. (1982) *J. Mol. Biol. 155*, 367–388. Williamson, M. P. (1990) *Biopolymers 29*, 1423–1431.
Wishart, D. S., Sykes, B. D., & Richards, F. M. (1991) *J. Mol. Biol. 222*, 311–333.
Wishart, D. S., Sykes, B. D., & Richards, F. M. (1992) *Biochemistry 31*, 1647–1651.
Wright, P. E., Dyson, H. J., & Lerner, R. A. (1988) *Biochemistry 27*, 7167–7175.
Wüthrich, K. (1986) *NMR of proteins and nucleic acids*, J. Wiley and Sons, New York.